Chinese Journal of Catalysis 43 (2022) 2259–2269

available at www.sciencedirect.com

ScienceDirect

journal homepage: www.sciencedirect.com/journal/chinese-journal-of-catalysis

Article

Conversion of methanol to propylene over SAPO-14: Reaction mechanism and deactivation

Ye Wang [a,b], Jingfeng Han [a], Nan Wang [a,c], Bing Li [a], Miao Yang [a,*], Yimo Wu [a,c], Zixiao Jiang [a,c], Yingxu Wei [a], Peng Tian [a], Zhongmin Liu [a,#]

[a] *National Engineering Research Center of Lower-Carbon Catalysis Technology, Dalian Institute of Chemical Physics, Chinese Academy of Sciences, Dalian 116023, Liaoning, China*

[b] *Green Catalysis Centre, College of Chemistry, Zhengzhou University, Zhengzhou 450001, Henan, China*

[c] *University of Chinese Academy of Sciences, Beijing 100049, China*

ARTICLE INFO

Article history:
Received 28 February 2022
Accepted 22 April 2022
Available online 20 June 2022

Keywords:
Methanol to propylene
SAPO-14 molecular sieve
UV Raman spectroscopy
Dual-cycle mechanism
Deactivation

ABSTRACT

Methanol to olefins (MTO) reaction as an important non-oil route to produce light olefins has been industrialized, and received over 80% ethylene plus propylene selectivity. However, to achieve high single ethylene or propylene selectivity towards the fluctuated market demand is still full of challenge. Small-pore SAPO-14 molecular sieve is a rare MTO catalyst exhibiting extra-high propylene selectivity. It provides us a valuable clue for further understanding of the relationship between molecular sieve structure and MTO catalytic performance. In this work, a seconds-level sampling fixed-bed reactor was used to capture real-time product distributions, which help to achieve more selectivity data in response to very short catalytic life of SAPO-14. Changes in product distribution, especially during the low activity stage, reflect valuable information on the reaction pathway. Combined with *in situ* diffuse reflectance infrared Fourier-transform spectroscopy, *in situ* ultraviolet Raman measurements and $^{12}C/^{13}C$ isotopic switch experiments, a reaction pathway evolution from dual cycle to olefins-based cycle dominant was revealed. In addition, the deactivation behaviors of SAPO-14 were also investigated, which revealed that polymethylbenzenes have been the deactivated species in such a situation. This work provides helpful hints on the development of characteristic methanol to propylene (MTP) catalysts.

1. Introduction

Methanol to olefins (MTO) reaction as a successful alternative route for producing ethylene and propylene from the nonoil resources like coal, natural gas and biomass, is highly valuable for oil deficiency countries (regions) to supply basic petrochemicals [1–3]. Over the past decade, the MTO process has been industrialized based on SAPO-34 catalyst and fluidized bed reactor [4]. Although the selectivity of light olefins is over 80% in SAPO-34 catalyzed MTO process, the produced propylene to ethylene (P/E) ratio is close to 1, and the adjustable range is narrow [5]. In order to meet the frequently fluctu-

* Corresponding author. E-mail: yangmiao@dicp.ac.cn
# Corresponding author. E-mail: liuzm@dicp.ac.cn

This work was supported by the National Natural Science Foundation of China (22171259, 21991090, 21991091, 22172166), the Innovation Research Foundation of Dalian Institute of Chemical Physics, Chinese Academy of Sciences (DICP I201909) and Youth Innovation Promotion Association CAS (2021182).
DOI: 10.1016/S1872-2067(22)64123-8 | http://www.sciencedirect.com/journal/chinese-journal-of-catalysis | Chin. J. Catal., Vol. 43, No. 8, August 2022

ated market requirements, it is highly desirable to develop characteristic MTO catalyst or process to achieve high single ethylene or propylene selectivity together with high total olefins yield.

Selectivity regulation has always been a very critical yet challenging goal of heterogeneous catalysis. To control the selectivity of MTO reaction, considerable efforts have been devoted to understanding the relationship between MTO reaction and structures/properties of zeolite [6–12]. The structure and acidity of zeolite catalyst are considered the two most important characteristics affording selectivity control, which determine directly the formed hydrocarbon pool species (HCPs) and MTO reaction route [13–15]. Besides, products diffuse out of zeolite catalyst *via* window shape selection where the passing of C_{4+} products will be restricted more seriously by smaller 8-ring pore openings. So, small-pore SAPO molecular sieves show obvious superiority for the production of light olefins. Most of the small-pore SAPO molecular sieves have nanosized cavity structures which can accommodate highly active intermediates in large volume such as polymethylbenzenium (polyMB$^+$) and polymethylcyclopentadienium (polyMCP$^+$) cations, and favor aromatics-based cycle [9,16,17]. Such reaction route gives priority to ethylene production, coupled with the contribution of olefins-based cycle, the final P/E ratios will be in the 0.5–2 range. Modifying the dual cycle ratio over small-pore molecular sieve catalyst to break through the P/E ratio limitation remains a challenge.

M. Davis *et al*. recently described the cage size of small-pore molecular sieves with the concept of cage-defining ring, and correlated this feature to light olefin product distribution and MTO activity [18]. Among the 30 different zeolitic and $AlPO_4$-based microporous materials with 14 topologies, ERI (6.76 × 6.73 Å) and LEV (7.15 × 6.84 Å) have the smallest cage-defining ring sizes, which are close yet smaller than the 12-ring pore size of the GME molecular sieve (7.0 × 7.0 Å). The MTO reaction catalyzed by them produces more C_2H_4 than C_3H_6. When the cage-defining ring size increases to 12–14 rings like DDR, AEI and SAV topologies, C_3H_6 is more selective than C_2H_4 with the highest P/E ratio of ca. 2.0. Further increasing the cage-defining ring sizes to 16-ring (larger than 10 Å, like LTA and RHO), the selectivity of C_4H_8 becomes the highest with irregular P/E ratios. Conversely, zeolites with 8-ring channels but more condensed structures, such as SAPO-39 (ATN), MCM-35 (MTF), ERS-7 (ESV) and RUB-37 (CDO), have been reported to be inactive for the MTO reaction [19]. It suggests that a reaction space (cage size) larger than 8-ring dimension might be necessary to catalyze MTO reaction. Unlike the above-mentioned results, we recently synthesized a silica-containing AlPO-14 molecular sieve (AFN), which has ultra-small cage and elliptical narrow 8-ring pore openings [20]. It can catalyze methanol conversion effectively with unprecedentedly high propylene selectivity up to 77.3%. According to the proposed classification by M. Davis, the cage-defining ring size of AFN topology is 6.84 × 5.17 Å, which lies between the 10-ring and 12-ring pore sizes (Fig. 1). Little attention has been paid to such structure before, which can provide us with a valuable example to acquire deeper insight into the relationship between molecular sieve structure and MTO catalytic performance.

In this work, the MTO catalytic performance of the SAPO-14 molecular sieve was investigated to better understand the reaction nature. A self-made fixed-bed reactor equipped with multi-valve storage was used to monitor product selectivity, especially during the short-lasting low activity stage. *In situ* diffuse reflectance infrared Fourier-transform spectroscopy (DRIFTS) and ultraviolet (UV) Raman spectroscopy, combined with $^{12}C/^{13}C$ isotopic methanol switch experiments, were applied to study evolution of the reaction pathway. In addition, the coke deposition and deactivation processes were investigated through various *ex-situ* techniques, and the utilization efficiency of methanol carbon atom conversion was evaluated. A clear reaction path of methanol conversion on SAPO-14 has

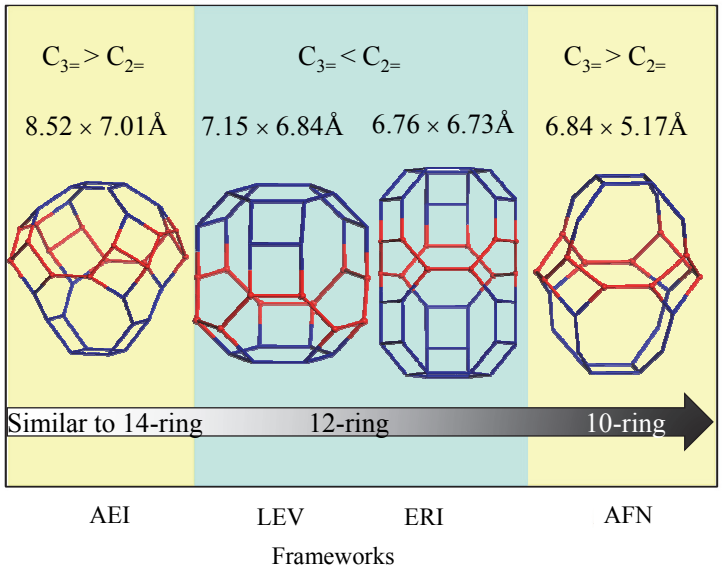

Fig. 1. The views and sizes of cage-defining rings (red colored) for AEI, LEV, ERI, and AFN topologies.

been figured out, which provides useful information for the design and development of structure-function-related MTO catalysts.

2. Experimental

2.1. Catalytic

2.1.1. Self-made seconds-level sampling fixed-bed reaction

The MTO reaction was carried out in a self-made seconds-level sampling fixed-bed reactor with a quartz tube with inner diameter of 2 mm at atmospheric pressure. The reaction steps are as follows: 0.1 g catalyst (40–60 mesh) was loaded in the tubular reactor, and then activated at 873 K for 0.5 h in He atmosphere. Afterward, the reaction temperature was adjusted to 673 K. At the same time, flowing He was bubbled through methanol at a flow rate of 11.2 mL/min at 277.2 K, which afforded a weight hourly space velocity (WHSV) of 0.5 h^{-1}. Samples of the gas mixtures after reaction at 10, 15, 20, 30, 40, 60, 90, 120, 180, 360, 1200, 2400, 3600 s were taken *via* a valve (Vici valco instruments), and each of them was saved in one of 13 quantitative rings, which were kept at constant 393 K before analysis. The time on stream (TOS) is calculated by deducting 40 s gas travelling time from the reactor to the gas chromatography. The compositions were analyzed by an online gas chromatograph (Agilent GC 7890B) with a flame ionization detector (FID) and a HP-Plot/Q+PT column (30 m × 0.32 mm × 20 μm).

2.1.2. Collection of the spent catalysts after fixed-bed MTO reaction

SAPO-14 catalysts, exposed to methanol (WHSV of 0.5 h^{-1}) for different MTO reaction time (6, 37, 139 and 207 minutes, respectively), were collected to investigate the deactivation process. The operation details of every collection were as follows: 0.2 g catalyst (40–60 mesh) was first loaded in a stainless steel tubular reactor with inner diameter of 6 mm, and the catalyst was then activated at 773 K in an N_2 flow of 40 mL/min for 0.5 h. Afterward, the reaction temperature was decreased to 673 K. The methanol was fed by passing N_2 carrier gas at a flow rate of 29.5 mL/min through a saturator containing methanol at 274 K, corresponding to a WHSV of 0.5 h^{-1}. The reaction was stopped at the desired TOS. The gas mixtures were analyzed by an online gas chromatograph (Agilent GC 7890B) with an FID and a CP-PoraPLOT Q-HT column (27.5 m × 0.32 mm × 10 μm). The spent catalyst in the reactor was quickly removed and evenly mixed after liquid nitrogen cooling, while waiting for further characterizations including TG analyses and N_2 adsorption measurements. Since the amount of coke can be estimated, the calculation of carbon resource utilization efficiency is based on this set of MTO data. In the calculation, methanol and dimethyl ether (DME) were regarded as reactants, and the MTO results are listed in Table S1.

2.2. In situ DRIFT spectra

In situ DRIFT spectra were collected on a Bruker Tensor 27 instrument supplied with a MCT detector. The catalyst powder was charged in a diffuse reflectance infrared cell with ZnSe window which can work at high temperatures and high pressures. The absorbance spectra were obtained by collecting 16 scans at 4 cm^{-1} resolution. Before the adsorption of reactants, the sample was first calcined in N_2 stream flowing 20 mL/min at 773 K for 150 min. Subsequently, the catalyst was cooled down to adsorption temperature in N_2 stream, and the spectrum of catalyst was recorded as reference. After that, methanol was fed by passing the carrier gas (N_2, the purity is 99.999%) through a methanol saturator maintained at 673 K into the reactor. Meanwhile, the reaction time was recorded, and the spectrum was collected every 30 seconds.

2.3. In situ UV Raman spectra

UV Raman spectra were recorded using a home-made single stage UV Raman spectrograph with a spectral resolution of 2 cm^{-1}. The single-frequency UV laser line at 244 nm was from an efficient external cavity frequency doubler (Wavetrain, Spectra-Physics) of the single-frequency laser at 488 nm laser (Genesis, CX 488, Coherent). The exciting source was with an output of 10 mW and the power of the laser at the sample was about 2.0 mW.

For *in situ* UV Raman experiments, the catalyst sample was calcined in air at 873 K before the reaction. Then, the feed gas (He, 99.99%) was passed through a homebuilt methanol bubbler at 277.2 K. For the *in situ* isotope exchange experiment using ^{13}C-methanol, *in situ* UV Raman spectra were collected during an isotope switching experiment. ^{13}C-methanol reaction was first introduced in SAPO-14 catalyst bed at 673 K for 6 min, and then the reactant was switched to ^{12}C-methanol reaction.

2.4. Characterizations of the spent catalysts

Thermogravimetric analysis (TGA) was measured on a TA SDTQ 600 analyzer with a temperature-programmed rate of 10 K/min in air from 298 to 1173 K. And the loss between 573 and 1073 K was used to estimate the total coke content.

The Brunauer-Emmett-Teller theory (BET) surface area and micropore volume were determined by N_2 adsorption-desorption on a Micromeritics ASAP 2020 system. The total surface area was calculated based on the BET equation. The micropore volume was evaluated using the t-plot method. In the sample pretreatment, the fresh catalyst was treated in a vacuum at 623 K for 4 h, and the deactivated catalysts were treated in a vacuum at 363 K for 1 h followed by 3 h at 473 K. This can completely remove the adsorbed water, while avoiding the decomposition of coke.

A modified HF dissolution-solvent extraction method was used to extract carbonaceous deposits from discharged catalysts. 50.0 mg of deactivated catalysts were dissolved in 0.5 mL of 20% HF solution in a Teflon vial. Allow time for the catalyst to dissolve fully and the carbonaceous species extracted with 0.5 mL of tetrachloromethane (CCl_4) with hexachloroethane C_2Cl_6 (50 ppm) as interior label. The CCl_4 solution was identified by the gas chromatography-mass spectrometry (GC-MS) using the Agilent 7890A Gas Chromatograph equipped with a

HP-5 capillary column and an FID detector after separation.

To further prove the identification of the coke species. The ultraviolet-visible (UV-vis) spectrum was collected on Varian Cary 5000 UV-Vis-NIR spectrophotometer and $BaSO_4$ was used as a reference. Matrix-assisted laser desorption/ionization Fourier-transform ion cyclotron resonance mass spectrometry (MALDI FT-ICR MS) measurements were conducted to further identify the larger carbonaceous deposit. Two methods were used for sample preparation and analysis, namely direct measurement of the deactivated samples with MALDI FT-ICR MS and measurement of the extract on the same equipment as the deactivated catalyst measurement. Specific operation methods refer to reference [21].

2.5. Carbon resource utilization efficiency

Carbon resource utilization efficiency is defined as the conversion efficiency of methanol into target light olefin products including ethylene, propylene and C_4 products. Only the data in highly active period are selected since the catalyst is supposed to be used in fluidized bed technology. The conversion and selectivity were calculated on CH_2 basis. DME was considered as reactant in the calculation. The average conversion $\bar{\alpha}$ and selectivity $\bar{S}$ data of 3, 20 and 37 min were used to calculate carbon resource utilization efficiency. Since part of the carbon atoms of methanol stay in solid catalyst as coke deposition besides the gaseous products, the absolute molar yield of each light olefin product is estimated by considering the coke deposition. The molar amount of gas products is evaluated by subtracting the carbon in coke from fed methanol within 37 min. The yield of CO and CO_2 has been proved to be negligible by gas chromatography (GC) analysis. The amount of coke is estimated based on the results of TG analysis. Carbon resource utilization efficiency is thus can be calculated by the following Equation (1).

$$C_{\text{resource utilization efficiency}}(\%) = (\bar{S}_{C2H4} + \bar{S}_{C3H6} + \bar{S}_{C4}) \times \bar{\alpha} \times (C_1 - C_2) \div C_1 \quad (1)$$

where C_1 is the total carbon moles of methanol. C_2 is the moles of coke deposition estimated by TG and assuming that the molecular formula of coke deposition is $(CH)_n$.

The turnover frequency is further calculated by Equation (2) which reflects the amount of target products obtained per unit time and per acid site over a catalyst.

$$\text{Turnover frequency} = C_1 \times C_{\text{resource utilization efficiency}} \div A \div T \quad (2)$$

where A is the acid amount of the catalyst. T is the reaction time.

3. Results and discussion

3.1. Seconds-level products analysis of MTO reaction on SAPO-14

SAPO-14 and a reference sample SAPO-18 with comparable Si content were prepared according to our previous work [20], and their physicochemical properties were provided in supporting information (Figs. S1–S3). Both samples possess good

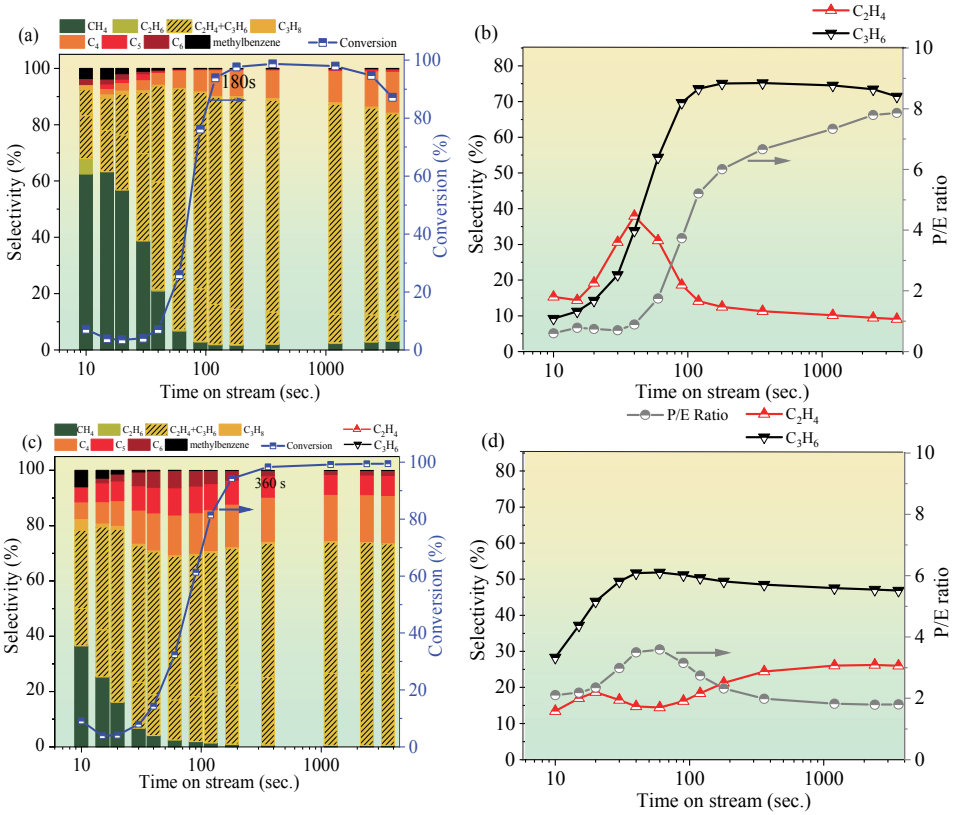

Fig. 2. Seconds-level MTO product distribution and conversion and selectivity profiles of propylene, ethylene and propylene/ethylene ratios over SAPO-14 (a,b) and SAPO-18 (c,d). Reaction condition: 673 K, weight hourly space velocity: 0.5 h^{-1}, methanol partial pressure: 5 kPa.

crystallinity and low acid density (0.25 mmol/g for SAPO-14 and 0.20 mmol/g for SAPO-18, determined by NH_3-TPD of Fig. S4). Their MTO catalytic performances were first tested by employing a self-made fixed bed reactor with a seconds-order sampling function to achieve real-time product distribution details [22]. As seen in Fig. 2(a), the methanol conversions over SAPO-14 present S-shape curves. The methanol conversion is quite low before TOS of 40 s ranging from 3.5% to 7.1%. Methane is a main product at this stage which gradually decreases with the increased yield of light olefins. The decomposition and hydrogenolysis reactions of methanol reaction might be more serious over "narrow" SAPO-14, resulting in methane product [23]. Besides, a small amount of methylbenzene appears together with methane suggesting the occurrence of olefins aromatization and aromatics alkylation. It implies that the HCPs are forming and accumulating in the AFN cage of SAPO-14 at the very initial stage. This is important for the subsequent initiation of the autocatalysis process. The conversion rises sharply when autocatalysis is launched, which climbs to 97.7% with 87.5% selectivity of ethylene plus propylene at 180 s. C_4 products account for only 9.2%, while C_5 and C_6 products are less than 0.5%. This should thank to the small 8-ring windows of SAPO-14 with more stringent diffusion restriction for C_{4+} products. Notably, the propylene selectivity increases rapidly from initial 9.2% at 10 s to 75.1% at 180 s, which keeps over 70% until the end of the reaction (Fig. 2(b)). Such results are very rare which is highly attractive for methanol to propylene process. Correspondingly, the ethylene selectivity first increased from the initial 15.3% to 37.9% at 40 s and then decreased sharply to 12.5% at 180 s. The selectivity curves of ethylene and propylene resemble each other before TOS ≤ 40 s, which move in opposite directions afterwards. The P/E ratio (Fig. 2(b)) ranges from 0.6 to 0.9 before 40 s, and then rises monotonously to around 7.8. These results suggest that the catalytic behavior of SAPO-14 in the initial stage might be similar to that of small-pore large-cage SAPO catalyst, which then becomes quite different.

For comparison, a similar MTO catalytic evaluation was performed on SAPO-18 molecular sieve with a comparable Si content of 2.0%, as shown in Figs. 2(c) and 2(d). It takes about double time for SAPO-18, 360 s *vs.* 180 s of SAPO-14, to launch its autocatalysis. Sufficient HCP compounds need to be accumulated before they start to play an important role [24]. The AEI cage of SAPO-18 is much larger than that of SAPO-14, which can accommodate more active aromatic species with larger sizes. It is therefore reasonable to see the longer startup time needed for SAPO-18. In addition, the catalytic lifetime of SAPO-18 is obviously longer than SAPO-14, which thanks to the much better diffusion ability of SAPO-18 than SAPO-14. The reactants convert more easily at the acidic sites of SAPO-18, where the formed products leave in time to avoid side reactions or coke deposition. Because of this, the products distribution and their change trends on SAPO-18 are obviously different from those on SAPO-14. The methane selectivity is relatively low initially with more olefins products, and the selectivities of ethylene and propylene show a relatively slight fluctuation. It is noted that propylene is always more selective than ethylene with a P/E ratio curve ranging from 1.8 to 3.6 (Fig. 2(d)). The P/E ratio reaches a maximum when the conversion is 32.4% at TOS of 60 s, which gradually decreases to ca. 2.0 as the progress of the reaction. The previous $^{12}C/^{13}C$-methanol isotopic switch experiments have confirmed that aromatics-based cycle is a main reaction route at the high activity period of SAPO-18 catalyzed MTO reaction [13]. Besides, olefins-based cycle has also been demonstrated to be important by periodic density functional theory calculations despite the insufficient direct experimental evidence [25]. Considering that the aromatics-based cycle delivers both ethylene and propylene, while the olefins-based cycle mainly produces propylene, it is believed that the P/E ratio of 3.6 in the low conversion period is contributed by both aromatics-based and olefins-based cycles. When the autocatalysis process starts up, the dual cycle converts to aromatics-based cycle dominant, and the P/E ratio of 1.8 mainly results from the formation of highly substituted methylbenzenes offering the higher reaction activity and favoring the formation of more propylene.

After comprehensive analysis of the selectivity changes of the above two catalysts, the spatial confined effect was considered to be the most important reason for their selectivity differences. On the one hand, due to the limited reaction space for SAPO-14, the decomposition and hydrogenolysis reactions of methanol are strengthened, leading to higher methane selectivity of SAPO-14. On the other hand, small AFN cages should severely inhibit the aromatics-based cycle before autocatalysis launching, where the HCPs concentration comes to a maximum and ethylene selectivity begins to decline sharply. Combined with the strict shape-selection by pore-openings, the propylene selectivity increased steadily while the C_{4+} products are difficult to diffusion out resulting in an extra-high propylene yield finally.

3.2. *In situ DRIFTs studies of MTO conversion*

In situ DRIFTs spectra were measured to observe the species changes over the SAPO-14 catalyst during the methanol conversion. As shown in Fig. 3, two infrared (IR) peaks at 2977

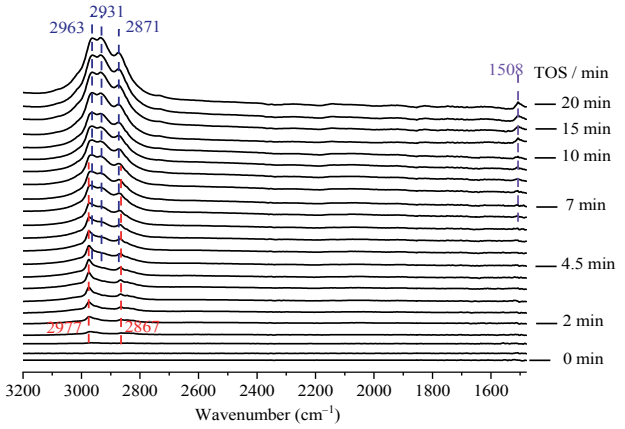

Fig. 3. *In situ* diffuse reflectance infrared Fourier-transform spectra recorded during methanol conversion over SAPO-14 at 673 K. The spectra were recorded from 0 to 20 min.

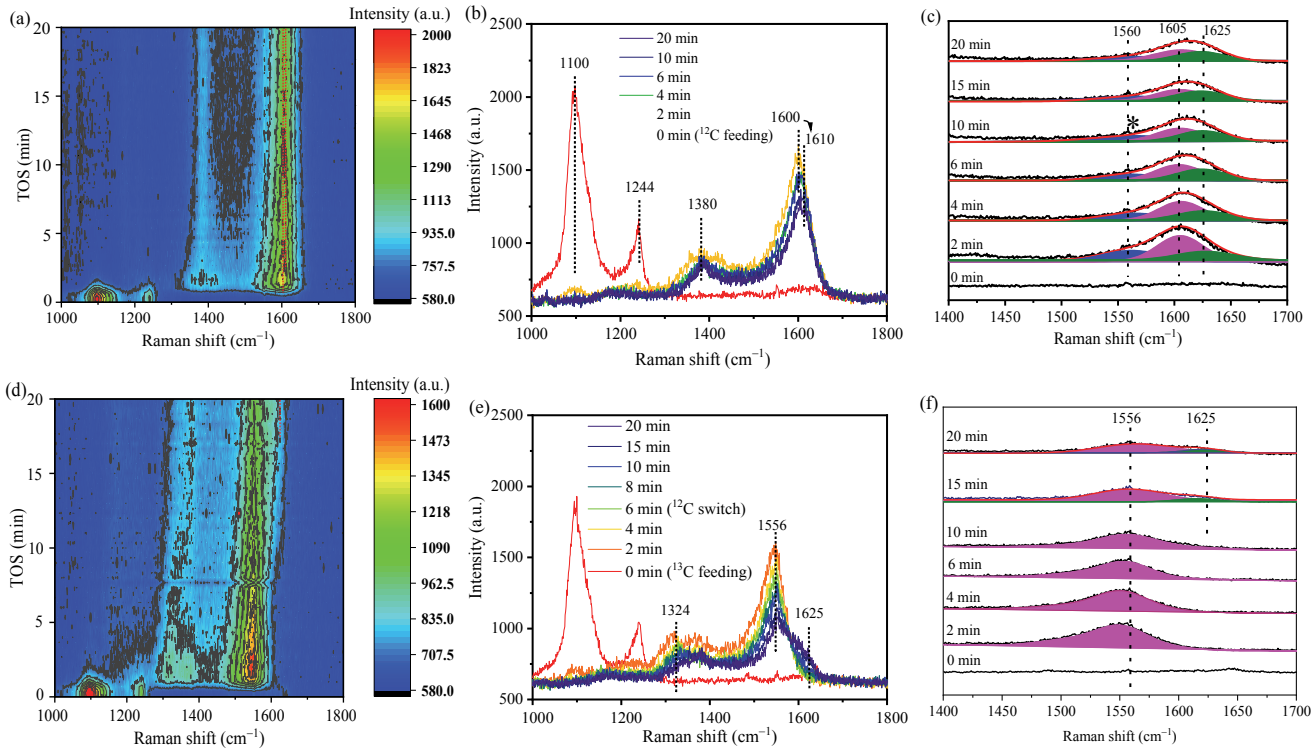

Fig. 4. Time-resolved UV Raman spectra, the selected typical UV Raman spectra and their peak fittings of SAPO-14 catalyst in ^{12}C-methanol conversion (a–c), and ^{13}C-methanol conversion followed by ^{12}C-methanol switch at a TOS of 6 min (d–f). Reaction condition: 673 K; methanol partial pressure: 5 kPa; ultraviolet excitation line: 244 nm.

and 2867 cm^{-1} appeared gradually with the introduction of methanol. The peaks shift to 2963 and 2871 cm^{-1} as the reaction proceeds with two new peaks appearance at 2931 and 1508 cm^{-1}. According to the literature, 2977 and 2867 cm^{-1} are attributed to the stretching vibration peaks of methyl C-H of surface methoxy species (SMS) [26–28]. The signals of 2963, 2931, and 2871 cm^{-1} can be attributed to olefins species [29,30]. The weak signal of 1508 cm^{-1} might be related to the dimethylcyclopentenyl (DMCP) cationic species [30]. It is believed that SMS is rapidly formed at the beginning of the reaction. As the reaction proceeds, olefins species form gradually accompanied by its cyclization reaction, which replace SMS to occupy the active sites of the molecular sieve and become the active HCPs. Notably, there is not aromatic species signal (1615 cm^{-1}) can be detected in the first 20 min [28,31]. This may be due to the low coke capacity of small-pore structure of SAPO-14. It is also not excluded that the absence of aromatic species ascribed to the insufficient sensitivity of IR spectroscopy.

3.3. *In situ* UV Raman studies of MTO conversion

In situ UV Raman spectra of catalyst bed surface were measured by a self-made UV Raman system with a fast scanning rate of 20 s and a low laser power of ca. 2 mW. This makes it possible to detect changes of MTO reaction details in real time sensitively and prevent burning effects [32,33]. The time-resolved UV Raman spectra of SAPO-14 before and after interaction with methanol at 673 K were shown in Fig. 4(a), and the selected data with more details were shown in Figs. 4(b) and 4(c). The fresh catalyst shows two strong bands at 1100 and 1244 cm^{-1} related to the framework vibration of SAPO-14. Upon touching methanol, the two signals vanish and another two new Raman bands appear at ca. 1380 and 1600 cm^{-1}. The wide band at 1380 cm^{-1} is related to the C-H bending or breathing vibrations of aromatic rings [34]. The broad band at around 1600 cm^{-1} is an overlapped result of various organic species which can be fitted as a combination of 1560, 1605 and 1625 cm^{-1} as shown in Fig. 4(c). The small sharp band at 1560 cm^{-1} is the characteristic Raman band of oxygen in the optical path outside the reactor. The band at 1605 cm^{-1} is related to aromatic carbocation while that at 1625 cm^{-1} are ascribed to olefin species [35–37]. They correspond to the HCP species for aromatics-based and olefins-based cycles, respectively. The characteristic band at 1605 cm^{-1} declines initially and then stabilizes gradually, while the band at 1625 cm^{-1} remains almost unchanged in the whole process. So, the overall Raman signals present an apparent blue shift from 1600 to 1610 cm^{-1} with TOS as seen in Fig. 4(b). The results indicate that aromatics-based cycle has been restricted.

Isotopic switch experiment combined with *in situ* UV Raman spectroscopy was further employed to clarify the reaction route (Fig. 4(d)). When ^{13}C-methanol was fed as the starting reactant, the UV Raman bands appeared at 1324 and 1556 cm^{-1} in contrast to those of 1380 and 1600 cm^{-1} for ^{12}C-methanol feeding. According to the investigation of ^{12}C/^{13}C switch in MTO

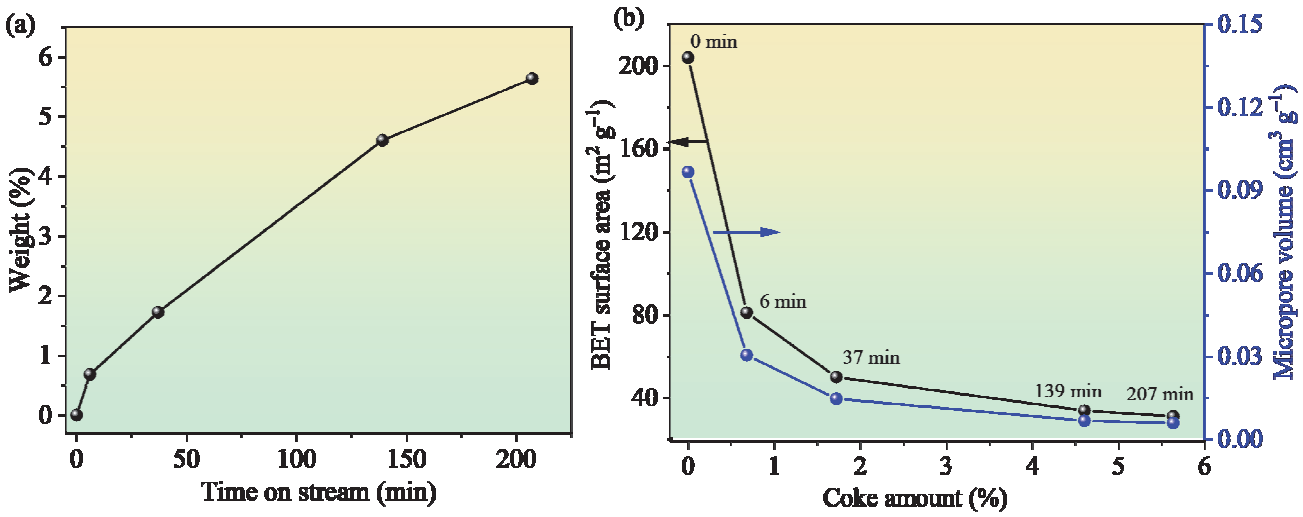

Fig. 5. The coke amount as a function of time on stream (a). The micropore volume (blue line) and Brunauer-Emmett-Teller (BET) surface area (black line) of spent SAPO-14 catalysts as functions of coke amount (b).

reaction by An *et al.* [37], the UV Raman signal of ^{13}C-labelled aromatic carbocation exhibited a red shift from 1605 to 1560 cm^{-1}. However, the position of olefins carbocation for ^{13}C-methanol conversion is not identified. Thus, it is difficult to deconstruct the band of 1556 cm^{-1} for the moment. Remarkably, after ^{13}C-methanol was switched to ^{12}C-methanol at a TOS of 6 min, a newly-appeared band at ca. 1625 cm^{-1} was gradually formed, as seen in Figs. 4(e) and 4(f), which was ascribed to the ^{12}C-olefins species. This indicates that olefins-based cycle is highly active in the methanol conversion process, while the aromatic species (the band at 1556 cm^{-1} after $^{13}C/^{12}C$ switch) serve like "coke" on the catalyst. The *in situ* UV Raman spectroscopy combined with $^{13}C/^{12}C$ isotopic switch experiment confirm that the MTO reaction process over SAPO-14 catalyst is dominated by olefins-based cycle.

3.4. Deactivation process and coke identification

To investigate the deactivation process, SAPO-14 catalysts were exposed to methanol for different time (WHSV = 0.5 h^{-1}), and then were analyzed by TG and N_2 adsorption measurements. As seen in Fig. S5, the samples in the first 37 minutes were almost colorless, indicating that there was not much carbon deposition on the outer surface of the catalyst. As the reaction time is prolonged to 139 min, the darker color of the unloaded catalyst was, suggesting the deeper degree of the MTO reaction. The weight loss between 573 and 1073 K in TG analysis was attributed to the combustion of the deposited coke (Fig. S6), and the amount of carbon deposition with reaction time was illustrated in Fig. 5(a) and Table S2. The coke deposition was almost negligible (0.7 wt%) at TOS of 6 min, which reached 1.7 wt% at 37 min, and 5.6 wt% at 207 min. The average coke formation rate (R_{coke} = coke amount/time on stream) was calculated to be 3.3 mg/h. The low number is due to low WHSV, the weaker acidity and smaller reaction space of SAPO-14. Notably, the micropore volume of SAPO-14 decreased sharply from 0.096 to 0.03 cm^3/g at TOS of 6 min and to 0.015 cm^3/g at 37 min (Fig. 5(b)). The loss of micropore volume was more than 60% after explosion in methanol for 6 min, although the coke deposition was only 0.7 wt% at this time. The fast loss of micropore volume suggests that the formed organics intermediate has blocked the channels of SAPO-14 molecular sieve. Comparatively, the decline of micropore volume for SAPO-34 is very slow in the initial stage which gets faster as the accumulation and growth of HCP species (Fig. S7) [38]. The large reaction space for CHA structure has larger coke capacity and therefore longer lifetime.

To identify the deactivation species, *ex situ* UV-vis spectroscopy and GC-MS analysis were further conducted. As shown in Fig. 6(a), the UV-vis spectra show broad and gradually intensified UV absorption peaks at around 270 nm indicating the presence of more and more benzene, naphthalene and their derivatives [39,40]. A very weak absorption peak at 326 nm is associated with the formation of tiny anthracene which might form on the surface of SAPO-14 catalyst. Notably, there is a broad peak at above 420 nm attributed to the presence of four condensed aromatic rings [39]. The result suggests that some large carbon species might be formed even the reaction space of SAPO-14 is quite narrow.

GC-MS analyses (Fig. 6(b)) show that polymethylbenzenes are the main species at TOS of 6 and 37 min. Combined with the N_2 adsorption result, it is believed that polymethylbenzenes have become the deactivated carbon. The formation of coke species larger than phenanthrene is not to be detected under the current condition. The carbonaceous deposits were further analyzed by MALDI FT-ICR MS. MALDI FT-ICR MS, as a powerful tool, has been used to identify the nature of coke species over a variety of zeolite catalysts [21,41,42]. As seen in Figs. 6(c) and S8, the peak positions of all the samples were basically the same, which consisted of two fragment ion groups with m/z

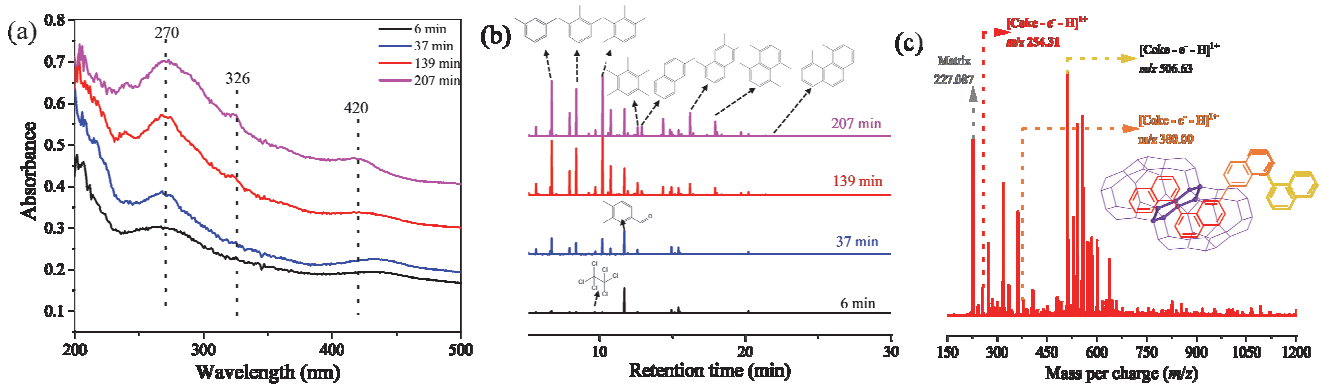

Fig. 6. Ultraviolet-visible spectra of SAPO-14 at different reaction times (a). Gas chromatography-mass spectrometry chromatograms of organic species in SAPO-14 at different reaction times (b). Matrix-assisted laser desorption/ionization Fourier-transform ion cyclotron resonance mass spectra for extracts obtained from SAPO-14 and the deduced possible molecular structure of polycyclic aromatic hydrocarbons (c). The indicated molecular structures are representative examples of possible structures. Reaction conditions: 673 K for 37 min; weight hourly space velocity: 0.5 h^{-1}.

ranges of 250–360 and 510–650 Da. The results show that the coke with larger molecular weight may be formed. The MS peak of 254.31, 380.00 and 506.63 Da correspond to the molecular weights of two, three and four naphthalene rings respectively. Moreover, the direct MALDI FT-ICR MS testing of deactivated SAPO-14 samples without HF treatment ruled out the possibility of carbon residue deposition on the external surface (Fig. S9). These results indicate that the cage-passing growth forming cross-linked multicore polycyclic aromatic hydrocarbons (PAHs) is also possible for SAPO-14. Coke across cages has been proved to exist widely in molecular sieve catalysts with cage structure close to each other. Checking the structure of AFN found that the AFN cages are connected by sharing 8 rings (inset of Fig. 6(c)), which allows the formation of large hydrocarbons by passing through the cages. With the deepening of the reaction, the coke species gradually grow up and the diffusion path is blocked completely, resulting in the complete deactivation.

3.5. *Carbon resource utilization efficiency*

The conversion efficiency of methanol on SAPO-14 catalyst was evaluated according to the method in section 2.5. The corresponding MTO catalytic data of the related SAPO catalysts are given in Table S1 and S3. Based on these data and formula (1) in section 2.5, the carbon resource utilization efficiency of SAPO-14 is calculated to be 74% (at T = 673 K and WHSV = 0.5 h^{-1}). Although this number is less than that of SAPO-34 (about 82% at 673 K and WHSV=2.0 h^{-1}) [43], the corresponding propylene yield of 58% on SAPO-14 is clearly superior than that on SAPO-34 (40%). Meanwhile, the turnover frequency of SAPO-14 was calculated to be about 0.013 s^{-1} (at T = 673 K and WHSV = 0.5 h^{-1}) based on the formula (2), which is comparable to that (ca. 0.016 s^{-1}) of SAPO-18 with the similar silica content. So, these results imply that SAPO-14 molecular sieve is a potential catalyst for methanol to propylene (MTP) reaction.

4. Conclusions

The methanol conversion process on SAPO-14 catalyst has been well studied by multiple *in situ* and *ex situ* techniques. A reaction route evolving from dual cycle to olefins-based cycle dominant was revealed, where the aromatics-based cycle was quickly inhibited by the small reaction space in SAPO-14 catalyst. The formed polymethylbenzenes were confirmed to be deactivated species blocking the channels and resulting in fast deactivation. An interesting question has ever been proposed on mechanistic understanding and selectivity control is that if the olefins-based cycle can run independently to maximize propylene selectivity. The present results indicate that the topology and acidity of SAPO-14 molecular sieve catalyst has been controlled to the critical point of catalyzing MTO reaction. The aromatics-based cycle can be effectively inhibited and an extra-high propylene selectivity is achieved with the assistance of orifice shape selection. However, the formation of aromatic species serving as deactivated species is inevitable thus far, which results in fast deactivation. Therefore, the synthesis of nanosized or hierarchical porous SAPO-14 to improve mass transfer and enlarge the coke capacity would be meaningful. Meanwhile, the strict shape-selective ability has to be well kept. More new molecular sieves with small window and cage sizes are also desirable to offer more options. By then, the fast deactivation will be further overcome by a circulating fluidized bed technique, and the new methanol-to-propylene catalyst is expected to be usable in industry.

Author contributions

All authors contributed to this work. All authors have given approval to the final version of the paper.

Declaration of Competing Interest

Graphical Abstract

Chin. J. Catal., 2022, 43: 0–0 doi: 10.1016/S1872-2067(22)64123-8

Conversion of methanol to propylene over SAPO-14: Reaction mechanism and deactivation

Ye Wang, Jingfeng Han, Nan Wang, Bing Li, Miao Yang *, Yimo Wu, Zixiao Jiang, Yingxu Wei, Peng Tian, Zhongmin Liu *
Dalian Institute of Chemical Physics, Chinese Academy of Sciences; Zhengzhou University; University of Chinese Academy of Sciences

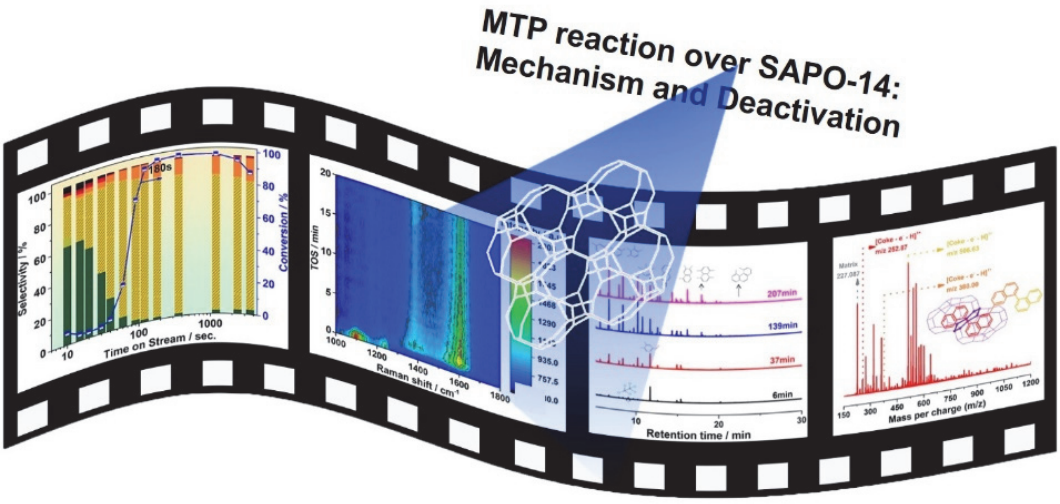

The reaction mechanism and deactivation process of methanol to propylene over SAPO-14 were investigated through various *in situ* and *ex situ* techniques, revealing the evolution of the reaction pathway from dual cycle to olefins-based cycle on SAPO-14.

The authors declare no competing financial interest.

Acknowledgments

We thank Dr. Wenna Zhang and Youming Ni for helpful discussion.

References

[1] M. Stöcker, *Microporous Mesoporous Mater.*, **1999**, 29, 3–48.
[2] J. Q. Chen, A. Bozzano, B. Glover, T. Fuglerud, S. Kvisle, *Catal. Today*, **2005**, 106, 103–107.
[3] I. Yarulina, A. D. Chowdhury, F. Meirer, B. M. Weckhuysen, J. Gascon, *Nat. Catal.*, **2018**, 1, 398–411.
[4] P. Tian, Y. X. Wei, M. Ye, Z. M. Liu, *ACS Catal.*, **2015**, 5, 1922–1938.
[5] M. Yang, D. Fan, Y. X. Wei, P. Tian, Z. M. Liu, *Adv. Mater.*, **2019**, 31, 192181.
[6] B. P. C. Hereijgers, F. Bleken, M. H. Nilsen, S. Svelle, K. -P. Lillerud, M. Bjorgen, B. M. Weckhuysen, U. Olsbye, *J. Catal.*, **2009**, 264, 77–87.
[7] S. Teketel, U. Olsbye, K. -P. Lillerud, P. Beato, S. Svelle, *Microporous Mesoporous Mater.*, **2010**, 136, 33–41.
[8] U. Olsbye, S. Svelle, M. Bjørgen, P. Beato, T. V. W. Janssens, F. Joensen, S. Bordiga, K. P. Lillerud, *Angew. Chem., Int. Ed.*, **2012**, 51, 5810–5831.
[9] J. Z. Li, Y. X. Wei, J. R. Chen, S. T. Xu, P. Tian, X. F. Yang, B. Li, J. B. Wang, Z. M. Liu, *ACS Catal.*, **2015**, 5, 661–665.
[10] P. Ferri, C. G. Li, C. Paris, A. Vidal-Moya, M. Moliner, M. Boronat, A. Corma, *ACS Catal.*, **2019**, 9, 11542–11551.
[11] J. W. Zhong, J. F. Han, Y. X. Wei, Z. M. Liu, *J. Catal.*, **2021**, 396, 23-31.
[12] S. Wang, Z. K. Li, Z. F. Qin, M. Dong, J. F. Li, W. B. Fan, J. G. Wang, *Chin. J. Catal.*, **2021**, 42, 1126–1136.
[13] J. R. Chen, J. Z. Li, C. Y. Yuan, S. T. Xu, Y. X. Wei, Q. Y. Wang, Y. Zhou, J. B. Wang, M. Z. Zhang, Y. L. He, S. L. Xu, Z. M. Liu, *Catal. Sci. Technol.*, **2014**, 4, 3268–3277.
[14] I. Pinilla-Herrero, U. Olsbye, C. Marquez-Alvarez, E. Sastre, *J. Catal.*, **2017**, 352, 191–207.
[15] S. S. Gao, Z. Q. Liu, S. T. Xu, A. M. Zheng, P. F. Wu, B. Li, X. S. Yuan, Y. X. Wei, Z. M. Liu, *J. Catal.*, **2019**, 377, 51–62.
[16] J. Z. Li, Y. X. Wei, J. R. Chen, P. Tian, X. Su, S. T. Xu, Y. Qi, Q. Y. Wang, Y. Zhou, Y. L. He, Z. M. Liu, *J. Am. Chem. Soc.*, **2012**, 134, 836–839.
[17] W. N. Zhang, J. R. Chen, S. T. Xu, Y. Y. Chu, Y. X. Wei, Y. C. Zhi, J. D. Huang, A. M. Zheng, X. Q. Wu, X. J. Meng, F. S. Xiao, F. Deng, Z. M. Liu, *ACS Catal.*, **2015**, 8, 10950–10963.
[18] J. H. Kang, F. H. Alshafei, S. I. Zones, M. E. Davis, *ACS Catal.* **2019**, 9, 6012–6019.
[19] M. A. Deimund, J. E. Schmidt, M. E. Davis, *Top. Catal.*, **2015**, 58, 416–423.
[20] M. Yang, B. Li, M. B. Gao, S. F. Lin, Y. Wang, S. T. Xu, X. B. Zhao, P. Guo, Y. X. Wei, M. Ye, P. Tian, Z. M. Liu, *ACS Catal.*, **2020**, 10, 3741–3749.
[21] N. Wang, Y. C. Zhi, Y. X. Wei, W. N. Zhang, Z. Q. Liu, J. D. Huang, T. T. Sun, S. T. Xu, S. F. Lin, Y. L. He, A. M. Zheng, Z. M. Liu, *Nat. Commun.*, **2020**, 11, 1079–1091.
[22] J. W. Zhong, J. F. Han, Y. X. Wei, S. T. Xu, T. T. Sun, S. Zeng, X. W. Guo, C. S. Song, Z. M. Liu, *Chin. J. Catal.*, **2019**, 40, 477–485.
[23] W. P. Zhao, B. Z. Zhang, G. R. Wang, H. C. Guo, *J. Energy Chem.*,

2014, 23, 201–206.
[24] L. Qi, Y. X. Wei, L. Xu, Z. M. Liu, *ACS Catal.*, **2015**, 5, 3973–3982.
[25] C. M. Wang, Y. D. Wang, Z. K. Xie, *Chin. J. Catal.*, **2018**, 39, 1272–1279.
[26] S. M. Campbell, X.-Z. Jiang, R. F. Howe, *Microporous Mesoporous Mater.*, **1999**, 29, 91–108.
[27] T. R. Forester, R. F. Howe, *J. Am. Chem. Soc.*, **1987**, 109, 5076–5082.
[28] X. Q. Wu, S. T. Xu, Y. X. Wei, W. N. Zhang, J. D. Huang, S. L. Xu, Y. L. He, S. F. Lin, T. T. Sun, Z. M. Liu, *ACS Catal.*, **2018**, 8, 7356–7361.
[29] I. B. Minova, S. K. Matam, A. Greenaway, C. R. A. Catlow, M. D. Frogley, G. Cinque, P. A. Wright, R. F. Howe, *ACS Catal.*, **2019**, 9, 6564–6570.
[30] S. F. Lin, Y. C. Zhi, W. Chen, H. Li, W. N. Zhang, C. Y. Lou, X. Q. Wu, S. Zeng, S. T. Xu, J. P. Xiao, A. M. Zheng, Y. X. Wei, Z. M. Liu, *J. Am. Chem. Soc.*, **2021**, 143, 12038–12052.
[31] S. S. Shao, H. Y. Zhang, R. Xiao, X. H. Li, Y. X. Cai, *J. Anal. Appl. Pyrolysis*, **2017**, 127, 258–268.
[32] D. S. Wragg, R. E. Johnsen, M. Balasundaram, P. Norby, H. Fjellvåg, A. Grønvold, T. Fuglerud, J. Hafizovic, Ø. B. Vistad, D. Akporiaye, *J. Catal.*, **2009**, 268, 290–296.
[33] D. Rojo-Gama, M. Signorile, F. Bonino, S. Bordiga, U. Olsbye, K.P. Lillerud, P. Beato, S. Svelle, *J. Catal.*, **2017**, 351, 33–48.
[34] M. Signorile, D. R. Gama, F. Bonino, S. Svelle, P. Beato, S. Bordiga, *Catal. Today*, **2019**, 336, 203–209.
[35] C. L. Angell, *J. Phys. Chem.*, **1973**, 77, 222–227.
[36] N. Sheppard, D. M. Simpson, *Q. Rev. Chem. Soc.*, **1952**, 6, 1–33.
[37] H. Y. An, F. Zhang, Z. H. Guan, X. B. Liu, F. T. Fan, C. Li, *ACS Catal.*, **2018**, 8, 9207–9215.
[38] S. S. Gao, S. T. Xu, Y. X. Wei, Q. L. Qiao, Z. C. Xu, X. Q. Wu, M. Z. Zhang, Y. L. He, S. L. Xu, Z. M. Liu, *J. Catal.*, **2018**, 367, 306–314.
[39] K. Y. Lee, H. -J. Chae, S. -Y. Jeong, G. Seo, *Appl. Catal., A*, **2009**, 369, 60–66.
[40] W. L. Dai, G. J. Wu, L. D. Li, N. J. Guan, M. Hunger, *ACS Catal.*, **2013**, 3, 588–596.
[41] L. Pinard, S. Hamieh, C. Canaff, F. F. Madeira, I. Batonneau-Gener, S. Maury, O. Delpoux, K. B. Tayeb, Y. Pouilloux, H. Vezin, *J. Catal.*, **2013**, 299, 284–297.
[42] N. Chaouati, A. Soualah, M. Chater, M. Tarighi, L. Pinard, *J. Catal.*, **2016**, 344, 354–364.
[43] Y. X. Wei, C. Y. Yuan, J. Z. Li, S. T. Xu, Y. Zhou, J. R. Chen, Q. Y. Wang, L. Xu, Y. Qi, Q. Zhang, Z. M. Liu, *ChemSusChem*, **2012**, 5, 906–912.

SAPO-14催化的甲醇制丙烯反应：反应机理与失活

王　冶[a,b], 韩晶峰[a], 王　男[a,c], 李　冰[a], 杨　淼[a,*], 吴一墨[a,c], 江子潇[a,c], 魏迎旭[a], 田　鹏[a], 刘中民[a,#]

[a]中国科学院大连化学物理研究所, 低碳催化技术国家工程研究中心, 辽宁大连116023
[b]郑州大学化学学院, 绿色催化中心, 河南郑州450001
[c]中国科学院大学, 北京100049

摘要: 甲醇制烯烃(MTO)反应作为重要的非石油路线生产低碳烯烃途径, 其乙烯加丙烯的选择性可高达80%以上. 然而, 由于乙烯和丙烯的收率接近, 如何调控单乙烯或丙烯的选择性以满足市场波动需求仍充满挑战. 小孔SAPO-14分子筛是本课题组最近报道的一种具有AFN拓扑结构的新型MTO催化剂, 其单程的丙烯选择性可超过70%, 丙烯/乙烯比为4–8. 研究SAPO-14分子筛的MTO催化机制、揭示其高丙烯选择性背后的原因, 有助于深入理解分子筛结构和物性与MTO催化性能之间的关联规律, 还将为开发新型甲醇制丙烯(MTP)催化剂提供新思路.

本文采用秒级采样固定床反应器对催化反应的选择性进行了监测, 结合原位红外光谱、原位紫外拉曼光谱和$^{12}C/^{13}C$甲醇切换实验研究反应路径演变. 还通过多种非原位表征手段考察了SAPO-14的失活过程, 对甲醇碳资源利用效率进行评估, 为设计和开发特色MTP催化剂提供理论依据.

产物分布变化, 特别是低活性期的变化可以反映出甲醇转化反应路径的一些重要信息. 从秒级采样固定床的反应结果可以看出, SAPO-14催化的MTO反应初期主要产物是甲烷. 随着自催化反应的启动, 甲烷选择性开始下降, 丙烯的选择性迅速上升, 达到70%以上并保持到反应结束. 反应前40 s, 乙烯与丙烯的选择性变化趋势相近, 40 s后乙烯选择性迅速降低、与丙烯选择性变化呈相反趋势. 相比之下, SAPO-18催化MTO反应时, 丙烯的选择性一直高于乙烯. 表明SAPO-14上的催化反应在40 s附近经历了巨大的转变. 而SAPO-18的反应路径相对平稳. 由于SAPO-14反应空间有限, 芳烃循环在自催化启动过程中受到了严重的限制, 因此乙烯的选择性呈现先增加后降低的趋势. 进一步通过原位紫外拉曼光谱和$^{12}C/^{13}C$甲醇同位素切换实验研究MTO反应细节. 当^{13}C甲醇切换成^{12}C甲醇后, 紫外拉曼光谱中只出现烯烃物种的信号, 证实了烯烃循环在SAPO-14的MTO反应过程中的主导性. 上述结果表明SAPO-14上的MTO反应路径经历了从双循环到烯烃循环为主的演变.

本文还利用多种表征手段研究了SAPO-14催化剂的失活行为. 氮气物理吸附结果表明, 随着积碳量的增加, SAPO-14催化剂的微孔孔容逐渐下降. 反应前6 min的孔容下降最快, 这说明反应初期形成的物种即可快速堵塞SAPO-14的孔道. 利用紫外可见光谱、气-质谱联用仪和傅里叶变换离子回旋共振质谱鉴定了反应中形成的积碳物种. 结果表明, 早期形成的多甲基苯物种即是失活物种, 另外还有可能形成跨笼积碳物种, 导致催化剂失活. 最后, 对甲醇的碳资源利用效率进行了评估, SAPO-14的碳资源利用效率为74%, 虽然低于SAPO-34的, 但是由于其较高的丙烯选择性, SAPO-14分子筛仍然是一个优秀的MTP催化剂.

烯烃循环和芳烃循环是否可以独立运转是MTO反应机理研究中一个有趣的问题. 如果可以最大限度地提升烯烃循环, 则有机会进一步提升丙烯选择性. SAPO-14分子筛的拓扑结构和酸性质已控制在可以催化MTO反应的临界点. 通过孔、笼择形, 可以有效地抑制芳烃循环, 实现丙烯的超高选择性. 但是芳烃物种的形成仍不可避免, 从而导致催化剂快速失活. 合成纳米级或多级孔SAPO-14, 从而改善其传质效率, 提升容碳能力, 将有助于制得更优的MTP分子筛催化剂.

关键词: 甲醇制丙烯; SAPO-14分子筛; 紫外拉曼光谱; 双循环机理; 失活

收稿日期: 2022-02-28. 接受日期: 2022-04-22. 上网时间: 2022-06-20.

*通讯联系人. 电子信箱: yangmiao@dicp.ac.cn

#通讯联系人. 电子信箱: liuzm@dicp.ac.cn

基金来源: 国家自然科学基金(22171259, 21991090, 21991091, 22172166); 中国科学院大连化学物理研究所创新研究基金(DICP I201909); 中国科学院青年创新促进会基金(2021182).

本文的电子版全文由Elsevier出版社在ScienceDirect上出版(http://www.sciencedirect.com/journal/chinese-journal-of-catalysis).